Velocity Mapping Toolbox (VMT): a processing and visualization suite for moving-vessel ADCP measurements

Journal:	*Earth Surface Processes and Landforms*
Manuscript ID:	ESP-11-0240.R2
Wiley - Manuscript type:	Paper
Date Submitted by the Author:	16-Oct-2012
Complete List of Authors:	Parsons, Daniel; University of Hull, Faculty of Science, Geography Jackson, Ryan; U.S. Geological Survey, Illinois Water Science Center Czuba, Jonathan; U.S. Geological Survey, Office of Surface Water Engel, Frank; University of Illinois, Geography Rhoads, Bruce; University of Illinois, Geography Oberg, Kevin; U.S. Geological Survey, Office of Surface Water Best, James; University of Illinois, Departments of Geology and Geography and Ven Te Chow Hydrosystems Laboratory Mueller, DAvid; U.S. Geological Survey, Office of Surface Water Johnson, Kevin; U.S. Geological Survey, Illinois Water Science Center Riley, James; University of Illinois, Geography
Keywords:	Flow, Velocity, Acoustic Doppler Current Profiler

Velocity Mapping Toolbox (VMT): a processing and visualization suite for moving-vessel ADCP measurements

[1*]Parsons, D.R., [2]Jackson, P.R., [3]Czuba, J.A., [4]Engel, F.L., [4]Rhoads, B.L., [5]Oberg, K.A., [6,4]Best, J.L., [7]Mueller, D.S., [2]Johnson, K.K., and [8]Riley, J.D.

[1]Department of Geography, Environment and Earth Sciences, Faculty of Science, University of Hull, HULL, HU6 7RX, UK. d.parsons@hull.ac.uk

[2]U.S. Geological Survey, Illinois Water Science Center, 1201 W. University Ave., Urbana, Illinois, 61801, USA.

[3]U.S. Geological Survey, Washington Water Science Center, 934 Broadway, Suite 300, Tacoma, WA 98402, USA.

[4]Department of Geography and Geographic Information Science, University of Illinois, Urbana, Illinois, 61801, USA.

[5]U.S. Geological Survey, Office of Surface Water, 1201 W. University Ave., Urbana, Illinois, 61801, USA.

[6]Departments of Geology, Mechanical Science and Engineering and Ven Te Chow Hydrosystems Laboratory, University of Illinois, Urbana, Illinois, 61801, USA.

[7]U.S. Geological Survey, Office of Surface Water, 9818 Bluegrass Parkway, Louisville, KY, 40299, USA.

[8]Department of Geology/Geography, Eastern Illinois University, Charleston, Illinois, 61920, USA.

Abstract

The use of acoustic Doppler current profilers (ADCP) for discharge measurements and three-dimensional flow mapping has increased rapidly in recent years and has been primarily driven by advances in acoustic technology and signal processing. Recent research has developed a variety of methods for processing data obtained from a range of ADCP deployments and this paper builds on this progress by describing new software for processing and visualizing ADCP data collected along transects in rivers or other bodies of water. The new utility, the Velocity Mapping Toolbox (VMT), allows rapid processing (vector rotation, projection, averaging and smoothing), visualization (planform and cross-section vector and contouring), and analysis of a range of ADCP-derived datasets. The paper documents the data processing routines in the toolbox and presents a set of diverse examples that demonstrate its capabilities. The toolbox is applicable to the analysis of ADCP data collected in a wide range of aquatic environments and is made available as open-source code along with this publication.

Any use of trade, product, or firm names is for descriptive purposes only and does not imply endorsement by the U.S. Government.

1.0 Introduction

Over the past 20 years, acoustic Doppler Current Profilers (ADCPs) have revolutionized the measurement of flow and discharge in open channels (cf. Gordon, 1989; Simpson and Oltman, 1993; Oberg and Mueller, 1994). The reliability and efficiency of ADCPs for obtaining accurate discharge measurements (Morlock 1996; Oberg and Mueller, 2007) are widely acknowledged and ADCPs are used routinely by many agencies and environmental consultants worldwide to measure and record discharge in inland waterways, rivers, lakes, and estuaries. In 2010, the U.S. Geological Survey (USGS) utilized hydroacoustic instrumentation for approximately 69% of all discharge measurements for stream gauging across the United States. Of these, approximately 82% of non-wading discharge measurements were made using ADCPs (Garcia et al., 2012).

Not only do ADCPs provide rapid, accurate measurements of discharges in flowing bodies of water, but these instruments also are increasingly being used in scientific research to characterize the spatio-temporal patterns of flow in various types of water bodies (e.g. Wagner and Mueller, 2001; Muste et al., 2004a; Jacobson et al., 2004; Dinehart and Burau 2005a,b; Parsons et al., 2005, 2007; Szupiany et al., 2009; Jackson et al., 2009; Czuba et al., 2011; Wright and Kaplinski, 2011; Riley and Rhoads, 2012). Indeed, the extensive three-dimensional velocity data provided by ADCPs allow for detailed characterization of complex flow fields in natural rivers and the relation of these flow fields to extant or changing channel boundaries (e.g. Parsons et al., 2005; Szupiany et al., 2009; Wright and Kaplinski, 2011; Riley and Rhoads, 2012). Recent applications and deployments of ADCPs have also shown how these instruments can yield data on turbulence characteristics (e.g. Droz et al., 1998; Stacey et al., 1999; Lu and Lueck, 1999; Nystrom et al, 2007), suspended sediment concentration dynamics (through use of acoustic backscatter) (e.g. Gartner, 2004, Kostaschuk et al., 2004, Dinehart and Burau, 2005a,b; Wall et al., 2006; Topping et al., 2006; Shugar et al., 2010), spatial variations in shear-stress (Sime et al., 2007), and bedload transport rates (through quantification of a moving bed condition and the differences detectable between the instrument-derived boat velocity from bottom track and GPS-derived boat velocity) (Rennie et al., 2002; Rennie and Millar, 2007; Jamieson et al., 2009) Thus, ADCPs have become multipurpose instruments for examining flow, morphology and sediment flux, thereby demonstrating considerable promise for improved process-based understanding of geophysical processes in a wide range of aquatic environments (Best et al., 2005; Parsons et al., 2005; Garcia et al., 2007; Bartholomä et al. 2009; French et al. 2008; Jackson et al. 2008; Lane et al. 2008; Kostaschuk et al. 2009, 2010; Shugar et al. 2010; Wright and Kaplinski, 2011).

The increasing use of ADCPs to explore the characteristics of complex natural flows has led to a need for post-processing methods for managing, evaluating, analyzing, and displaying three-dimensional velocity data. Methods for processing ADCP time series data from fixed bed (up-looking orientation) moorings (c.f. Côté et al., 2011; Donovan 2004) have been in existence for some time. A number of data processing techniques for moving-vessel deployments have been described and most involve collection of data along transects (e.g. Muste et al., 2004a; Dinehart

and Burau, 2005a,b; Szupiany et al., 2007, 2009). However, many of these methods are designed for singular purposes and have limited flexibility in their application. For example, Le Bot et al. (2011) present a methodology, called CASCADE, for extracting ADCP data collected in marine environments along vessel transects and outline a routine to derive spatially-averaged velocities along such transects. However, because ADCP data collected from single transects across an open-channel often contain substantial noise and variability, accurate characterizations of three-dimensional velocity patterns typically require compositing of data from repeat transects (Szupiany et al. 2007, 2009). Dinehart and Burau (2005a,b) presented a method in which multiple transects can be projected and averaged onto a 2D planar grid to allow analysis of the 3D flow field, whereas Rennie and Church (2010) developed a procedure whereby spatially-distributed ADCP data can be interpolated onto a planar-horizontal 2D grid covering large areas up to entire channel reaches. Although both of these methods hold significant promise, specifically in terms of aiding geomorphological interpretations of measured flow processes, the methods have been developed for specific applications and are not widely available to the earth-science community. A commercially-available tool, LOG_aFlow® (e.g. Müller et al., 2001), is available and allows for interpolation of ADCP-derived velocity onto 2D horizontal planes and 3D volumes using hydrodynamic interpolation in space and time. However this tool is not specifically designed for mapping of cross-section data, which are often used for analysis of morphodynamic and geomorphological flow processes (e.g. Dinehart and Burau, 2005a,b; Parsons et al., 2007; Szupiany et al., 2009). Kim et al. (2007) developed AdcpXP, a post-processing software package for ADCP data that includes spatial- and depth-averaging routines, in addition to scripts for computation of bulk flow parameters, turbulence parameters, and dispersion coefficients. A freely-available software tool, called VMS, includes analytical capabilities for quality assurance of moving-vessel, multiple-transect ADCP data, with the general aim of improving processing and visualization of large, reach-scale ADCP data sets for comparison with results of numerical and physical models (Kim et al., 2009). While useful, none of these ADCP data-processing packages computes three-dimensional velocity components, including components used to identify secondary flow, using techniques employed by the geomorphological process community. To this end, the need exists for an analytical technique for amalgamating velocity data from multiple ADCP transects to produce a composite depiction of three-dimensional velocity fields at channel cross-sections. Herein, we present a new software tool, the Velocity Mapping Toolbox (VMT), to address this need.

VMT is a Matlab®-based toolbox for processing, analyzing, and displaying cross-sectional velocity data collected along multiple ADCP transects. Input to VMT consists of ASCII output files from the ADCP data-collection software (Teledyne RD Instruments, 2009). The software projects data collected along several irregular ship tracks, or measurement transects, onto a straight-line plane that defines a measurement cross-section. The velocity data from individual transects are then averaged to produce a composite representation of the cross-sectional flow field. The

software can be used to explore patterns of three-dimensional fluid motion through several methods for calculation of secondary flows (e.g. Rhoads and Kenworthy, 1998; Lane et al., 2000), a defining feature of VMT setting it apart from other available software. The software also includes capabilities for analyzing the acoustic backscatter, bathymetric, and temperature data obtained from an ADCP. A user-friendly graphical user interface (GUI) enhances program functionality and provides ready access to two- and three-dimensional plotting functions, allowing rapid display and interrogation of velocity, backscatter, and bathymetry data. This paper describes the basic processing methods employed by VMT and highlights some of the capabilities of the toolbox through three example applications.

2.0 Acoustic Doppler Current Profilers (ADCP)

Detailed background information on the principles of acoustic Doppler current profilers can be found in Mueller and Wagner (2009), Simpson (2001), and Gordon (1996). In brief, the ADCP uses acoustic physics to measure the three-dimensional velocity of flowing water in fluvial, lacustrine, estuarine, coastal, and marine environments. It does so by transmitting an acoustic signal, at a known frequency, into the water column and recording the detectable acoustic backscatter from small particles suspended and carried within the flow field, and that are assumed to be moving at the same velocity as the water. The measurable Doppler shift in acoustic frequency (and/or the phase-amplitude of superimposed pulses) of this backscattered signal is then used to measure fluid velocity along the beam path. The backscatter signal received from the acoustic pulse traveling through the water column is gated over a range (time) to produce successive segments, called bins, along each of four (three in some systems) acoustic beams. Bins thus represent discrete measurement volumes for velocities at different depths over the water column. Because the individual beams are oriented in different directions, velocity components that are oriented orthogonally to one another can be measured under the assumption that water currents are uniform (homogeneous) across layers at a constant depth over the footprint of the acoustic beams. A trigonometric transformation is employed to compute three-dimensional velocity components within a Cartesian coordinate system. This process generates vertical profiles, or ensembles, of three-dimensional velocity components over the flow depth. The ensemble sampling rate is a function of the flow depth and frequency and configuration of the instrument, but can be as high as 5 Hz (many instruments sample at a higher frequency and internally average this data to reduce noise). ADCPs can be deployed at a fixed location (e.g. a surface mooring or a bed-mounted and up-looking configuration), whereby profiles of three-dimensional velocity are obtained as a time series, or from a moving vessel, whereby velocity data are collected as spatial transects (longitudinal or cross-sectional). This paper focuses on the latter application.

3.0 The Velocity Mapping Toolbox (VMT): An Overview

VMT is accessed through a graphical user interface (GUI) (Fig. 1) and is currently only capable of reading ADCP data files in ASCII format exported from WinRiver II data-collection software provided by the ADCP manufacturer Teledyne RD Instruments. Data files should be quality-assured using WinRiver II, or other software packages, and then imported into VMT as individual transects or, as is now often the case for velocity mapping (e.g. Szupiany et al., 2009), as groups of repeat transects for a single cross-section (Fig. 2). Presently (2012), VMT utilizes only measured velocity data in all computations and no attempt is made in VMT to account for unmeasured areas near the bed, surface, and transect edges.

Once the velocity data are pre-processed and quality assured in WinRiver II, they are imported into VMT as ASCII files and several computational steps are performed automatically (Fig. 3). First, either a mean cross-section orientation is calculated from data for a set of transects or, if the user prefers, this calculated cross-section can be replaced by a cross-section with a user-defined orientation and length (Fig. 3 – Step 1). The horizontal and vertical dimensions of an interpolation grid are then defined for the cross-section. In Step 2 (Fig. 3), velocity data from each individual transect are projected onto the cross-section using an anisotropic projection method and the projected data are interpolated onto the defined cross-section grid (Fig. 3 – Step 3). In this step, the user has the option to apply a correction to the observed velocities to account for potential streamwise variations in depth between locations of the observation points and the mapped points, assuming a constant streamwise mass flux (Hoitink et al. 2009). This simple correction scales the observed streamwise velocity in each bin by the ratio of the water column depth at the observation point and the depth of the mean cross-section at the projected observation point. The projected and interpolated velocity data for the set of transects are then averaged over the grid (Fig. 3 – Step 4), to produce a mean representation of the velocity field for the cross-section. Finally, the averaged three-dimensional velocity components for the cross-section are used to compute other metrics, such as the orientation and magnitude of velocity vectors and secondary flow by means of user-selectable methods. Once these computations are complete, a variety of user-defined options are available for smoothing and plotting the data. The following section describes each of these steps in detail.

4.0 VMT Data Averaging Routines

4.1 Defining an Average Cross-Section Orientation

Two methods can be used to define the orientation of a cross-section onto which data for individual transects will be mapped: 1) fitting of positions (UTM coordinates) of velocity profiles (ensembles) using least squares regression, and 2) using user-supplied UTM coordinates for endpoints of the cross-section. The first option is the default and is performed automatically unless the user specifies option two. When used with a global positioning system (GPS), as is normally

recommended for velocity mapping applications and discharge measurements with moving-bed conditions (e.g. Mueller and Wagner 2009), each vertical profile of three-dimensional ADCP velocity data, or ensemble, is automatically georeferenced during data collection. VMT transforms the recorded latitude and longitude coordinate data for each ADCP ensemble into an easting and northing in Universal Transverse Mercator (UTM) coordinates, automatically selecting the correct UTM zone. In the first method, the toolbox determines a mean cross-section orientation for a set of individual transects (ship tracks) by fitting a least squares regression line through the UTM positions of every ensemble in a set of transects (Fig. 2). Data are compiled from all repeat transects and the GPS positions of every ensemble (velocity profile) are used in the regression analysis to define a line that best represents the linear pattern of the data cloud (Fig. 2 and Fig. 3 – Step 1). The endpoints of the resulting cross-section are defined by the limits of the data cloud to ensure that the line spans the entire extent of the measured data. This method best represents the overall pattern of the set of ship tracks and is most appropriate when performing a single survey at a site.

When repeat surveys are conducted along a pre-determined line representing the cross-section, the user may wish to map velocity data onto this line to ensure that comparisons of velocity fields between different dates are consistent, i.e. that all the fields are mapped onto a plane with a fixed orientation relative to the channel alignment. Because the cross-section orientation produced by the best-fit method will vary slightly between surveys, no matter how accurate the boat navigation is, and because small differences in cross-section orientation can affect the magnitudes of secondary flows, using the fixed endpoints option might be preferable for comparing changes in three-dimensional flow structure between different measurement campaigns. However, care should be taken when using this method to ensure that projecting the repeat transects onto a user-defined cross-section is reasonable, given the position and alignment of the transects relative to the cross-section.

4.2 Defining the Interpolation Grid

The horizontal spacing of ensembles along each moving-vessel transect differs because of changes in boat speed. Moreover, ensembles in different transects are not usually spatially coincident. To overcome these issues, a uniform grid for interpolation of data is generated along the cross-section line (Fig. 2 and Fig. 3 – Step 1). The horizontal resolution of the grid is user-specified (default = 1 m) and the vertical resolution equals the vertical dimension of the ADCP bins (i.e. bin size). Whereas the cross-section defines the plane onto which data will be projected, the grid defines the nodes on this plane onto which data will be interpolated.

4.3 Projecting Transect Data onto the Plane of the Cross-Section

The next step in the transect-averaging procedure is to project data from individual transects onto the plane of the cross-section (Fig. 3 – Step 2). Virtually all ship tracks defining individual transects

are irregular and deviate both in position and length from the plane of the cross-section. Projection of the velocity vector data from the irregular transects onto the straight-line plane of the cross-section is accomplished through an orthogonal translation of the data point from its original location (*X,Y*) to a point on the cross-section line (X_{proj}, Y_{proj}). This orthogonal projection occurs along a line that is perpendicular to the cross-section line and passing through the data point of interest. The projected co-ordinates of a point on the mean cross-section for a point originally located at (*X,Y*) are given by

$$X_{proj} = \frac{X - mb + mY}{m^2 + 1} \qquad (1)$$

$$Y_{proj} = \frac{b + mX + m^2Y}{m^2 + 1} \qquad (2)$$

where *m* and *b* are the slope and intercept of the cross-section line. This transformation is completed for every ensemble in a transect, thereby projecting a dataset along an irregular ship track onto the straight line of the cross-section. This projection routine is repeated for every transect loaded into VMT for the cross-section under analysis. Users are responsible for ensuring that the loaded transects are representative of the cross-section and mapping of the data to the straight line of the cross-section is a valid assumption (including data in transects lying too far off the line that can result in the introduction of errors in reaches with variable bathymetry and flow distributions).

4.4 Interpolating Individual Transect Data to the User-Specified Grid Nodes

The next step is to interpolate projected data from individual transects onto the grid nodes in the cross-section. To accomplish this task, a linear interpolation scheme is applied to each individual transect (Fig. 3 – Step 3). Care must be taken when choosing the horizontal grid-node spacing to ensure this spacing is appropriate for the data set: choosing too large a grid node spacing will result in a coarse horizontal resolution of the velocity field, while choosing too small a spacing will lead to excessive interpolation where ensembles are widely-spaced. VMT defaults to a 1 m spacing and also automatically computes a recommended minimum grid node spacing, which equals the median plus one standard deviation of the projected ensemble spacing along the cross-section for all the transects. This recommendation is provided to help the user define an optimum grid node spacing for a data set.

4.5 Averaging the Transect Data at Each Grid Node

The projected and interpolated velocity data for all transects are averaged at every grid node in the cross-section to obtain a composite representation of the velocity field (Fig. 3 – Step 4). A simple

arithmetic mean is applied for each of the basic velocity components (east, north, and vertical velocities) and for acoustic backscatter and bed depth. After averaging is complete for all grid nodes, a coordinate rotation is applied to transform velocity components in basic (Earth) coordinates into velocity components in the plane of the cross-section. This transformation yields mean streamwise (U, positive downstream), cross-stream (V, positive to the left bank) and vertical (W, positive up) velocity components for every grid node. These velocity components, in turn, are used to compute two-dimensional velocity vector magnitudes and orientations for the set of grid nodes.

4.6 Rotation Schemes, Secondary Flow Vectors, and Depth-Averaged Velocities

Several coordinate rotation schemes are used in VMT to calculate different types of primary and secondary velocity components. The definitions of the primary and secondary velocity components depend on the rotation scheme used in the computation (see Lane et al., 2000 for a detailed explanation). All of these schemes involve rotating horizontal planes of the flow around the vertical axis of the cross-section. In no case is the vertical plane of the flow rotated around the horizontal axis; thus, W remains unchanged in these rotations. Initially the software rotates data collected by the ADCP in a northing-easting frame of reference into the plane of the cross-section. This scheme is referred to as the "no rotation" scheme and generates velocity components oriented orthogonal to the cross-section (U), parallel to the cross-section in the horizontal direction (V) and parallel to the plane of the cross-section in the vertical direction (W). The zero net secondary discharge method reorients the cross-section so that the net discharge in the lateral plane of the rotated cross-section equals zero (Markham and Thorne, 1992) to yield U_{zsd} and V_{zsd}. The Rozovskii method involves rotating each individual ensemble around its vertical axis to obtain zero net secondary discharge over the ensemble (Rozovskii, 1957) to yield U_{roz} and V_{roz}. The primary and secondary velocities derived from the Rozovskii method are also decomposed into downstream and cross-stream components of U_{roz} and V_{roz} relative to the orientation of the channel cross-section (Rhoads and Kenworthy, 1998).

The different types of secondary velocity components are used along with the vertical velocity component to compute the orientation and magnitude of the secondary flow vectors. The basic formulae for these computations are:

$$S_m = \sqrt{{L_c}^2 + W^2} \qquad (3)$$

$$S_\theta = \tan\left(\frac{W}{L_c}\right)^{-1} \qquad (4)$$

where S_m is the vector magnitude, S_θ is the vector orientation, W is the vertical velocity component and L_c is a lateral velocity component (V, V_{zsd}, or V_{roz}). Secondary flow vectors calculated using horizontal velocity components from various rotation methods provide different perspectives on the characteristics of secondary flow (Rhoads and Kenworthy, 1999; Lane et al., 2000).

VMT also has the capability to compute depth- and layer-averaged velocities. In both cases, the average is computed by

$$V_{LA} = \frac{1}{d_2 - d_1} \int_{d_1}^{d_2} v dz \qquad (5)$$

where V_{LA} is the depth- or layer-averaged velocity, v is the north or east component of velocity (averaged independently), and d_1 and d_2 are the lower and upper limits of the depth range used in averaging, respectively. For layer-averaging, the user specifies d_1 and d_2 in the VMT interface. For depth-averaging, inputs for d_1 and d_2 are left blank and VMT computes the average over the full depth of measured flow. A separate layer average, V_{LA}, is computed for the north component and the east component of velocity at each grid node and then the two components are used to compute the magnitude and direction of the two-dimensional, layer-averaged velocity vectors.

It is important to note that an ADCP cannot measure near the bed or near the surface because of side-lobe interference, transducer ringing, flow disturbance, and the ADCP immersion depth. VMT does not estimate velocities in these unmeasured zones by extrapolating velocity data to the bed or to the surface. Therefore, depth-averaging in VMT is performed only over the measured vertical extent of the data. If the combination of the ADCP configuration and site conditions allow only a limited portion of the total water column to be measured, the depth-averaged velocity from VMT may not be representative of the true depth-averaged velocity.

4.7 Spatial Averaging and Smoothing

Transect averaging is used to approximate temporal averaging when performing moving-boat ADCP measurements. This pseudo-temporal averaging represents an improvement over single passes, but averaged data often still contain uncertainties related to instrument noise and turbulent fluctuations in velocities that can obscure overall flow patterns, especially the patterns of secondary flow. Smoothing of the velocity data through spatial averaging can help reduce local variability in the data, so that overall patterns of fluid motion can be clearly discerned.

VMT allows the user to spatially-average data both in plan view as well as in cross-sections using a moving average and a user-specified window size. The spatial averaging (or smoothing) routines used within VMT are simple moving-averages that work in one (planform) and two (cross-section) dimensions (Fig. 4). The user has complete control of the window size for the spatial averaging. In the VMT interface, the user specifies the half window size, i.e. the number of grid nodes *n* on either side of a point to include in averaging (planform). Setting the smoothing window

parameter to a value of *n* will replace the velocity at a point with the average of the point and *n* neighbouring points on either side of the point. For plan-view plots, the averaging is applied in a cross-stream direction only (depth- or layer-averaging is applied in the vertical). For cross-section data, the user specifies both a horizontal smoothing window size, n_h, and a vertical smoothing window size n_v. Setting these parameters (n_h, and n_v) to zero results in no spatial averaging. The routines ignore missing/invalid data, and data near the edges are averaged using only the available data within the averaging window. The total width of an averaging window can be computed by multiplying the grid node spacing by twice the half window size.

4.8 Plotting Capabilities

VMT includes complete plotting capabilities for depicting ADCP data in planform and cross-sectional views. Planform views are used to depict depth- or layer-averaged flow vectors (depth averaged over the measured profile only). Cross-sectional views include colour-based contour plots of a variety of velocity, backscatter, and flow direction data with the capability to superimpose secondary velocity vectors on these plots (e.g. see later Fig. 10). The backscatter intensity data used in VMT are those exported from the data collection software (WinRiver II), which have been adjusted for beam spread and adsorption (Teledyne RD Instruments, 2009). VMT users should thus verify that the backscatter values computed and exported from the software are suitable for their application.

VMT provides numerous options for plotting, some of which are discussed in the examples shown below. VMT also automatically calculates values for all variables during data input; thus, once the data are loaded, analysis of flow patterns can proceed by selecting different combinations of variables to display on cross-sectional plots and by choosing different levels of smoothing for these plots. New plots are generated rapidly because the program does not have to compute any new variables to produce alternative displays of the data.

5.0 Results

Three example applications are presented to illustrate some of the capabilities of VMT. The three applications include processing and visualization of ADCP measurements from: i) the Upper St. Clair River, the primary outlet from Lake Huron (MI, USA); ii) the Wabash-Embarras River confluence (IL, USA); and iii) Clinton Lake (IL, USA). For reference, Table 1 contains the processing and visualization parameters entered in the VMT interface to generate the associated figures for each site. Minor editing of the figures outside of VMT has been completed for publication (e.g. addition of scale bars, section numbers, and labels).

5.1 Upper St. Clair River

The Upper St. Clair River is the primary outlet for Lake Huron, which drains the upper Great Lakes into the Lake St. Clair-Lake Erie system. A field survey was conducted during July 2 - July 25, 2008, using a 19-foot aluminum work vessel (*R/V Sangamon*) and was part of the International Upper Great Lakes study into the possible impacts of the St. Clair River on lake levels (see Czuba et al., 2011). The survey was conducted with a 1200 kHz ADCP mounted near the bow on the port side of the boat. The ADCP was integrated with a Leica System 1230 differential Global Positioning System (dGPS) that provided real-time kinematic (RTK) position information at a relative accuracy of 0.02 m at 5 Hz. A series of eighteen cross-sections were established for data collection and at least 6 ADCP transects were obtained at each cross-section.

A planform view of the depth-averaged velocity vectors through the reach for each of the 18 cross-sections highlights the convergence and acceleration of the lake outflow into the Upper St. Clair River, the development of a large region of flow separation on the east bank downstream of the main constriction (eastern side of cross-sections 9-12) and deceleration of the flow as the channel widens at the downstream end of the survey reach (Fig. 5). Detailed views of the three-dimensional flow within one of the cross-sections (cross-section 9) shows data for individual transects that have been interpolated and averaged onto a regular grid, and then spatially-averaged for 1, 2, 4, 6, and 8 transects using VMT. The resulting velocity vectors have been rotated to the cross-section orientation within VMT, giving primary flow and secondary flow based on the zero secondary discharge definition. The primary velocity (U_{zsd}) is shown as a colour contour plot (Fig. 6) and the arrows represent the magnitude and orientation of the secondary velocity vectors (V_{zsd}, W). The vertical scale of the plot is exaggerated to clearly visualize the velocity field and the number of secondary velocity vectors plotted has been constrained to avoid excessive clutter (using options available within the VMT interface).

The comparison of averaging based on different numbers of transects highlights the influence of additional information on patterns of secondary flow (Fig. 6). The plot of the data from a single transect contains considerable local variability in the pattern of secondary velocity vectors (Fig. 6a). For example, large coherent turbulent structures of similar magnitude and scale, yet opposite direction, were seen in transects 1 (Fig. 6a) and 6 (not shown individually) above the scour hole near the left bank. As additional transects are included in the averaging, the secondary flow field becomes increasingly visible (Fig. 6b-e) due to averaging of large-scale turbulent eddies (e.g. Muste et al., 2004a,b; Szupiany et al., 2007) and instrument noise recorded in each of the individual transects.

The appearance of velocity data within the side-lobe interference band (zone of missing data near the bed) at 290 m in the cross-section in Figure 6c-e results from the inclusion of transect 4 in the averaging process. Transect 4 deviated up to 30 meters downstream of the measurement section, and deeper water within the scour hole on the right bank (see Fig. 5 inset) led to deeper velocity measurements compared to the other transects. Velocity data imposing into the side-lobe band is a tell-tale sign of variable depths between transects and can result in the

introduction of error. Users should either omit the erroneous transects (as in Czuba et al. 2011) or carefully review the results using VMT (averaging data with and without the problem transect) to ensure that the inclusion of the data does not introduce significant error into the average velocity distribution. For the present example, the inclusion of transect 4 introduces some error into the average velocity distribution for this section primarily near the bed at about 290 m across the cross-section, but it does not significantly alter the overall pattern of secondary circulation. While the pattern of the secondary flow field remains relatively constant between the six-transect average (Fig. 6d) and eight-transect average (Fig. 6e), the sudden jump in magnitude of the secondary flows in the scour hole on the right bank (as illustrated by the vector field and the increase in the magnitude of the reference vector) is caused by the large magnitude of flow within the scour hole in transect 7 with significant secondary flows of up to 0.7 ms^{-1}. In general, stronger secondary flows were observed in the scour hole along the right bank in transects 4-8 compared to the first three transects. The apparent impingement of these secondary flow vectors upon the bed is due, in part, to the streamwise variation in depth combined with the topographic steering of flow into the scour hole oriented at 15 degrees to the cross-section (see Fig. 5 inset). The orientation of the scour hole is such that flows within this feature are steered at about 172 degrees (and down-slope into the hole), while the primary flow direction for the entire section is 197.3 degrees (using the zero net secondary discharge definition). For a primary flow velocity of 1 ms^{-1}, this 25.3 degree difference in flow direction is capable of producing secondary flows on the order of 0.47 ms^{-1} oriented toward the left bank (toward the inside of the bend). Therefore, topographic steering within the right bank scour hole can account for the 0.4 ms^{-1} observed secondary flows near the bed at 290 m across the section in Figure 5e. This example illustrates that users must exercise care when interpreting the results from VMT. Users must consider not only the three-dimensional nature of the flow when analyzing two-dimensional plots, but also consider the method used to compute secondary flows and the morphology and geometry of the channel. While a detailed investigation of the number of transects required to capture the time-averaged secondary circulation is beyond the scope of the present paper, VMT provides the capability to efficiently perform such an analysis.

Figure 5, produced by the VMT analysis, clearly shows the large zone of recirculating, separated, flow on the eastern bank (right side of the plot) and a zone of decelerating flow close to the right bank (left side of the plot), whereas the secondary flow vectors, highlighted in Figure 6, define divergent flow through the cross-section over a central bar. Depiction of such detail in the transect-averaged, three-dimensional, flow processes across the entire cross-section allows substantive conclusions to be drawn on the sediment transport processes in the upper St. Clair River and the linkages between the formation and migration of the mid-channel bar (Czuba et al., 2011). In particular, fluid motion in the scour hole on the right side of the cross-section, which represents the outside of a gentle bend where flow is accelerating (Fig. 5), is characterized by outward-directed flow near the surface and inward-directed flow near the bed – a sign of secondary

circulation. Complex, three-dimensional, patterns of fluid motion are also evident on the left side of the cross-section where a shear layer bounds the large separation zone along the eastern bank. Additionally, the secondary flow vectors define divergent flow through the section over a central bar.

5.2 Wabash-Embarras Confluence

The Embarras River joins the Wabash River along a gently curving section of the Wabash River, which forms the border between Illinois and Indiana, USA (Fig. 7a). Data were collected at this confluence on May 23, 2006, using an aluminum work boat with a bow-mounted 1200 kHz Rio Grande ADCP and Trimble Ag132 dGPS receiver. The data-collection campaign occurred as part of a research project examining the influence of changes in total discharge and momentum ratio of the two rivers on flow structure and bed morphology within large-river confluences. A total of eight cross-sections were surveyed though the reach, with 4 to 5 transects being measured at each cross-section. Bathymetric data from each of the four ADCP beams have been extracted from the ADCP data sets and corrected for heading, pitch and roll and georeferenced using the VMT bathymetry export option. These data were used to construct a bathymetric map of the confluence in ArcGIS, illustrating the value of VMT for rapid processing and integration of flow and morphology data for analysis of process-form interactions.

Patterns of depth-averaged velocity through the confluence without spatial averaging (Fig. 7a) and with spatial averaging (Fig. 7b; n = 1) display little to no difference. The effect of spatial averaging in this case is small, but plan view spatial averaging can have a large effect on the visualization of flows in shallow, low-velocity streams or lakes where data can be noisy (e.g. see later Fig. 11). The effect of spatial averaging is more pronounced when applied to velocity data in cross-sections (Fig. 7). At cross-section 4, despite averaging of four repeat transects, the pattern of secondary vectors for a Rozovskii rotation without spatial averaging is highly variable (Fig. 8a). Applying spatial averaging with the nearest-neighbor (i.e. n = 1 for horizontal and vertical smoothing windows) helps define the secondary flow pattern considerably (Fig. 8b). Further enhancement can be achieved by choosing smoothing parameters independently in the horizontal and vertical directions (n_h = 8, n_v = 2, Fig. 8c). For example, by choosing n_h =8 for the horizontal smoothing window, a spatial average over 8 grid points on either side of a point results in a 4 m smoothing window because the horizontal grid node spacing was 0.25 m (the vertical window size is defined by the bin size for the ADCP data and the vertical smoothing window parameter). In all cases, the spatial averaging is applied on the gridded data set prior to data reduction for plotting.

The use of different rotations of the velocity data can facilitate analysis of the three-dimensional fluid motion, especially at river confluences, where flow fields are complex (Fig. 9). At the Embarras River-Wabash River confluence, the pattern of secondary flow vectors with no data rotation (Fig. 9a) reveals the entry of relatively slow-moving flow on the right from the Embarras River into the Wabash River, which is deflected toward the left. Because of this flow deflection, the

cross-section is skewed in relation to the mean flow direction over much of the Wabash River, producing vectors oriented consistently toward the left bank. As VMT allows the user to quickly switch between displays of different types of secondary flow vectors by simply changing the plot variables, both the zero net discharge (Fig. 9b) and Rozovskii (Fig. 9c) methods can be easily applied, which define different patterns of secondary flow. In particular, the Rozovskii method is effective at revealing the development of large-scale secondary circulation at the confluence, characterized by opposing patterns of near-surface and near-bed fluid motion where the two flows meet on the right side of the cross-section (Fig. 9c). The VMT-derived results thus reveal the detailed three-dimensional flow patterns through the confluence and allow analysis of the interactions of the confluent flows, including the formation of helical motion and downwelling of fluid over the confluence scour (Fig. 9c).

VMT allows all velocity components to be plotted individually for analysis; moreover, scalars such as acoustic backscatter intensity can be plotted and overlaid by secondary flow vectors to examine possible relations between sediment concentration, related to backscatter intensity, and flow patterns (Fig. 10). The zone of strong downwelling on the right side of cross-section 4, illustrated by the pattern of secondary velocity vectors, corresponds well with the zone of negative vertical velocities as depicted by the colour scheme associated with contouring (Fig. 10a). A zone of high backscatter intensity, which may be indicative of high levels of suspended sediment transport (Dinehart and Burau 2005a,b), is associated with strong near-bed flow to the left within the Wabash River (Fig. 10b). On the right, the incoming flow from the Embarras River, which contains little suspended sediment and therefore has low values of backscatter intensity, can be seen mixing with the sediment-laden Wabash River.

5.3 Clinton Lake

Clinton Lake in central Illinois (USA) is a reservoir with a surface area of approximately 20.2 km^2 and serves as a cooling pond for Clinton Nuclear Power Station. Cooling water is withdrawn from the west arm of the lake at a rate of approximately 42.5 m^3s^{-1} and discharged into the east arm of the lake at a temperature approximately 20 degrees Celsius warmer than the intake temperature (Figure 11a). The cycling of water through the plant creates a continuous circulation in the lake from the discharge outfall back to the intakes. Waste heat is dissipated to the atmosphere and dispersed in the lake as the thermal plume spreads through the surface water. The circulation induced by the plant was measured in 2008 using a 1200 kHz Rio Grande ADCP and visualized using VMT to better understand the lake dynamics and thermal conditions in late summer under normal power-station operating conditions.

VMT was used to average repeat transects collected along cross-sections spaced approximately 600 m apart throughout the lake (Fig. 11). In addition, a stand-alone utility in the VMT toolbox (ASCII2GIS) was used to extract the georeferenced water temperature data from the ADCP (used by the ADCP for calculation of sound velocity). The temperature data were imported

into ArcGIS and gridded over the study domain using ordinary kriging. In order to capture the circulation patterns in the thermal plume, the upper 2.5 m of the water column was layer-averaged in VMT and treated separately from the remainder of the water column. Plan-view plots showing layer-averaged velocity vectors (with a vector spacing of 7.5 m) overlaid on the surface water temperature distribution are shown for a portion of Clinton Lake downstream of the thermal effluent outfall (Fig. 11a). The results reveal how an embankment traversing the lake constricts the circulation of the thermal plume through two relatively small openings that generate relatively high velocities (0.30 ms^{-1} surface velocity and 0.06 ms^{-1} depth-averaged velocity). Immediately downstream of the bridge openings, the plume hugs the north bank of the lake – a pattern that may be linked to above-average bank retreat observed along this shoreline (W. Hafiz, Exelon Corporation, personal communication). The plume then detaches from the north bank and meanders across the lake to the outside of the bend, following a similar path to the creek that once flowed through this river valley.

The power of layer-averaging in VMT is apparent when the pattern of flow in Clinton Lake below a depth of 2.5 m is examined (Figure 11b). As the thermal plume spreads through the lake, it grows in size by entraining ambient water. This entrainment is greatest where high velocities and turbulence help drive mixing, such as near the outfall and the bridge constrictions. In order to satisfy continuity, water entrained into the thermal plume is replaced by water from elsewhere in the lake, thus driving a deep circulation at the lake bottom. Cool, deep water is driven along the lake bed in a direction opposite to that of the plume-induced surface current, until it reaches the mixing zone at the bridge constriction where it is arrested and entrained into the surface current (Fig. 11b). Computing a depth-averaged velocity at Clinton Lake using ADCP data for the entire water column would not capture this deep circulation and would significantly reduce the magnitude of the true thermal plume velocities. VMT thus easily gives the user complete freedom to depth- or layer- average the data over either the full depth of the measured flow or any portion of the measured water column.

6.0 Summary and future developments

This paper details the Velocity Mapping Toolbox (VMT), a new freely-available (open-source) toolbox for the post-processing and visualization of ADCP data collected along single or multiple transects, and illustrates its capabilities using data for three case studies. The toolbox is available to download from the USGS Hydroacoustics Web pages (http://hydroacoustics.usgs.gov/movingboat/VMT/VMT.shtml). The basic processing steps in VMT include defining an average cross-section orientation, defining an interpolation grid, projecting ADCP data for individual transects onto the plane of the cross-section, interpolating data for individual transects onto the grid nodes, averaging data for multiple transects at the grid nodes, calculating secondary flow vectors and depth-averaged velocities, and data smoothing through spatial-averaging. Once processing is complete, a wide range of display options are available for

exploring in detail the three-dimensional patterns of fluid motion in complex natural environments. The toolbox should be useful for a wide range of applications where flow measurements are conducted along transects using ADCPs. Improvements and advanced processing extensions for VMT are currently (2012) under development that will improve data filtering, allow users to import data from a wide range of ADCPs, use the standard output from VMT to compute estimates of vorticity, shear velocity, bed shear stress, the longitudinal dispersion coefficient, and suspended sediment concentrations (with a sediment calibration option for acoustic backscatter). In addition, scripts that will allow spatial positioning of ADCP data collected without GPS and automated routines to interpolate missing data in ADCP files are also currently under evaluation. Future versions of VMT will incorporate some or all of these advanced capabilities and we anticipate that the user community, with access to the open source code, will contribute to the evolution of VMT over time.

Acknowledgements

DP and JB would like to thank the UK Natural Environment Research Council (NERC) for award of grants NER/A/S/2001/00445 and NER/B/S/2003/00243 that enabled the initial development of this code, and the World Universities Network for funding a research visit for DP to Illinois where the majority of the analysis was performed. DP also thanks NERC for his Fellowship funding (NE/C002636) that enabled further development of this research. The authors kindly acknowledge support of the USGS Office of Surface Water for funding the primary development of VMT and the many contributors to code who helped expand and improve the capabilities of this toolbox including those that shared their work via the Matlab Central File Exchange. Work on VMT by Bruce Rhoads, Frank Engel and Jim Riley was supported by National Science Foundation (NSF) grants BCS 04533 6, BCS 06229 6, and BCS 003622.

Resources

Both a compiled and open-source MATLAB version of VMT can be downloaded, with example datasets, from the USGS Hydroacoustics Web pages at:

http://hydroacoustics.usgs.gov/movingboat/VMT/VMT.shtml

References

Bartholomä A, Kubicki A, Badewien TH, Flemming BW. 2009. Suspended sediment transport in the German Wadden Sea-seasonal variations and extreme events. *Ocean Dynamics* **59**: 213-225. DOI 10.1007/s10236-009-0193-6

Best JL, Kostaschuk RA, Peakall J, Villard PV, Franklin M, 2005. Whole flow field dynamics and velocity pulsing within natural sediment-laden underflows. *Geology* **33**: 765-768. DOI: 10.1130/G21516.1

Côté JM, Hotchkiss FA, Martini M, Denham CR. 2011. Acoustic Doppler Current Profiler Data Processing System Manual, U.S. Geological Survey Open-File Report 00-458, v. 4, 51 pp.

Czuba JA, Best JL, Oberg KA, Parsons DR, Jackson PR, Garcia MH, Ashmore P. 2011. Bed morphology, flow structure, and sediment transport at the outlet of Lake Huron and in the upper St. Clair River. *Journal of Great Lakes Res*earch **37**: 480-493. DOI: 10.1016/j.jglr.2011.05.011

Dinehart RL, Burau JR. 2005a. Repeated surveys by acoustic Doppler current profiler for flow and sediment dynamics in a tidal river. *Journal of Hydrology* **314:** 1-21. DOI:10.1016/j.jhydrol.2005.03.019

Dinehart RL, Burau JR. 2005b. Averaged indicators of secondary flow in repeated acoustic Doppler current profiler crossings of bends. *Water Resources Research* **41**: W09405. DOI:10.1029/2005WR004050

Donovan JM. 2004. VPV—The velocity profile viewer user manual, U.S. Geological Survey Open-File Report 2004-1255, 62 pp.

Droz CJ, López F, Prendes H. 1998. Mediciones de Velocidades y Caudales con un ADCP en el Río Paraná. *XVII Congreso Nacional del Agua y II Simposio de Recursos Hídricos del Cono Sur*, Santa Fé, Argentina. August 1998. (In Spanish)

French JR, Burningham H, Benson T. 2008. Tidal and Meteorological Forcing of Suspended Sediment Flux in a Muddy Mesotidal Estuary. *Estuaries and Coasts* **31**: 843-859. DOI 10.1007/s12237-008-9072-5

Garcia, CM, Tarrab L, Oberg K, Szupiany R, Cantero MI. 2012. Variance of discharge estimates sampled using acoustic Doppler current profilers from moving boats. *Journal of Hydraulic Engineering* **138(8)***:* 684-694*.* DOI:10.1061/(ASCE)HY.1943-7900.0000558

García CM, Oberg KA, García MH. 2007. ADCP measurements of gravity currents in the Chicago River, Illinois. *Journal of Hydraulic Engineering* **133:** 1356–1366. DOI: 10.1061/(ASCE)0733-9429(2007)133:12(1356)

Gartner J. 2004. Estimating suspended solids concentrations from backscatter intensity measured by acoustic Doppler current profiler in San Francisco Bay, California. *Marine Geology* **211**: 169–187. DOI: 10.1016/j.margeo.2004.07.001

Gordon RL. 1996. Acoustic Doppler Current Profilers. Principles of Operation: A Practical Primer. Second Edition for Broadband ADCPs. RD Instruments, 57 pp.

Gordon RL. 1989. Acoustic measurement of river discharge. *Journal of Hydraulic Engineering* **115(7)**: 925-936. DOI:10.1061/(ASCE)0733-9429(1989)115:7(925)

Hoitink AJF, Buschman FA, Vermeulen B. 2009. Continuous measurements of discharge from a horizontal acoustic Doppler current profiler in a tidal river. *Water Resources Research* **45:** W11406. DOI:10.1029/2009WR007791

Jackson PR, Garcia CM, Oberg KA, Johnson KK, Garcia MH. 2008. Density currents in the Chicago River: Characterization, effects on water quality, and potential sources. *Science of the Total Environment* **401**: 130-143. DOI:10.1016/j.scitotenv.2008.04.011

Jackson, PR, Oberg KA, Gardiner N., Shelton J. 2009. Velocity mapping in the Lower Congo River: A first look at the unique bathymetry and hydrodynamics of Bulu Reach, West Central Africa. In: *Proceedings of the 6th IAHR Symposium on River, Coastal, and Estuarine Morphodynamics* (RCEM 2009), Universidas Nacional Del Littoral: Santa Fe, Argentina, 1007-1014.

Jacobson RB, Elliott CM, Johnson III HE. 2004. Assessment of shallow-water habitat availability in modified dike structures, lower Missouri River. U.S. Geological Survey Open-File Report 2004-1409, 18 pp.

Jamieson E., Rennie CD, Jacobson RB. 2009. Evaluation of flow structure and bed load velocity in the vicinity of a submerged wing dike in a large sand bed river. In *33rd Congress: Water Engineering for a Sustainable Environment*, International Association of Hydraulic Engineering and Research: Vancouver, B. C.; 1-8.

Kim D, Muste M, Mueller DS, Winkler M. 2009. A quick tutorial for using VMS. *U.S. Army Corps of Engineers, 68 pp. (*Online publication accessed October 15, 2012; http://chl.erdc.usace.army.mil/Media/1/1/2/0/VMS_quick_tutorial.pdf)

Kim D, Muste M, Weber L, Asaman R. 2007. Getting to know AdcpXP ADCP eXtended Processing: A tutorial for using AdcpXP. *IIHR- Hydroscience and Engineering, University of Iowa*, Iowa City, IA; 87 pp. (Online publication accessed October 15, 2012; http://www.iihr.uiowa.edu/wp-content/uploads/2012/06/AdcpXP-Manual-sm.pdf)

Kostaschuk RA, Villard PV, Best JL. 2004. Measuring velocity and shear stress over dunes with an acoustic Doppler profiler. *Journal of Hydraulic Engineering* **30**: 932–936. DOI: 10.1061/(ASCE)0733-9429(2004)130:9(932)

Kostaschuk RA, Shugar D., Best JL, Parsons DR, Lane SN, Hardy RJ, Orfeo O. 2009a. Suspended sediment transport and deposition over a dune: Río Paraná, Argentina. *Earth Surface Processes and Landforms* **34**: 1605-1611. DOI: 10.1002/esp.1847

Kostaschuk R, Best J, Villard PV. 2010. The influence of dunes on mixing in a migrating salt-wedge: Frasier River estuary, Canada. *Earth Surface Processes and Landforms* **35**: 460-465. DOI: 10.1002/esp.1928

Lane, SN, Bradbrook KF, Richards KS, Biron PM, and Roy AG. 2000. Secondary circulation cells in river channel confluences: Measurement artifacts or coherent flow structures? *Hydrological Processes* **4**: 2047– 2071. DOI: 10.1002/1099-1085(20000815/30)14:11/12<2047::AID-HYP54>3.0.CO;2-4

Lane SN, Parsons DR, Best JL, Orfeo O., Kostaschuk RA, Hardy RJ. 2008. Causes of rapid mixing at a junction of two large rivers: Rio Paraná and Rio Paraguay, Argentina. *Journal of Geophysical Research* **113:** F02024, DOI: 10.1029/2006JF000745

Le Bot P, Kermabon C, Lherminier P, Gaillard F. 2011. CASCADE V6.1: Logiciel de validation et de visualisation des mesures ADCP de coque. *Rapport technique OPS/LPO 11-01. Ifremer, Centre de Brest*, France: 93 pp.

Lu Y, Lueck RG. 1999. Using a Broadband ADCP in a Tidal Channel. Part I: Mean Flow and Shear. *Journal Atmospheric and Oceanic Technologies* **6**: 1556–1567. DOI: 10.1175/1520-0426(1999)016<1556:UABAIA>2.0.CO;2

Markham AJ, Thorne, CR. 1992. Geomorphology of gravel-bed rivers. In *Dynamics of Gravel-bed Rivers,* Billi P, Hey RD, Thorne CR, Tacconi P (eds). Wiley and Sons: Chichester; 433-450.

Morlock SE. 1996. Evaluation of Acoustic Doppler Current Profiler Measurements of River Discharge. U.S. Geological Survey Water-Resources Investigations Report 95-4218. 41 pp.

Mueller DS, Wagner CR. 2009. Measuring discharge with acoustic Doppler current profilers from a moving boat: U.S. Geological Survey Techniques and Methods 3A–22. 72 pp.

Müller V, Eden H, Vorrath, D. 2001. LOG_aFlow®- the Hydraulic Software for Hydraulic Engineering and Navigation. In *Proceedings of the International Conference on Port and Maritime R&D and Technology*, 29.-31.10.2001, Shankar NJ, Cheong TA, Pengzhi L (eds). Singapore; 953 – 957.

Muste M, Yu K., Spasojevic M. 2004a. Practical Aspects of ADCP Data Use for Quantification of Mean River Flow Characteristics: Part I: Moving-Vessel Measurements. *Flow Measurement and Instrumentation* **15**: 1-16. DOI: 10.1016/j.flowmeasinst.2003.09.001

Muste M, Yu K, Pratt T, Abraham D. 2004b. Practical Aspects of ADCP Data Use for Quantification of Mean River Flow Characteristics: Part II: Fixed-Vessel Measurements. *Flow Measurement and Instrumentation* **15**: 17-28. DOI: 10.1016/j.flowmeasinst.2003.09.002

Nystrom EA, Rehmann CR, Oberg KA. 2007. Evaluation of Mean Velocity and Turbulence Measurements with ADCPs. *Journal of Hydraulic Engineering* **133**: 1310-1318. DOI: 10.1061/(ASCE)0733-9429(2007)133:12(1310)

Oberg KA, Mueller DS. 1994. Recent applications of Acoustic Doppler Current Profilers. In *Proceedings of Fundamentals and Advancements in Hydraulic Measurements and Experimentation*, ASCE: Reston, VA; 341–350.

Oberg KA, Mueller DS. 2007. Validation of streamflow measurements made with acoustic Doppler current profilers. *Journal of Hydraulic Engineering* **33**: 1422-1432. DOI:10.1061/(ASCE)0733-9429(2007)133:12(1421)

Parsons DR, Best JL, Orfeo O, Hardy RJ, Kostaschuk RA, Lane SN. 2005. The morphology and flow fields of three-dimensional dunes, Rio Paraná, Argentina: results from simultaneous

multibeam echo sounding and acoustic Doppler current profiling. *Journal of Geophysical Research* **110**: F04S03. DOI: 10.1029/2004JF000231

Parsons DR, Best JL, Lane S.N, Orfeo O, Hardy RJ, Kostaschuk RA. 2007. Form roughness and the absence of secondary flow in a large confluence-diffluence, Rio Paraná, Argentina. *Earth Surface Processes and Landforms* **32**: 155-162. DOI: 10.1002/esp.1457

Rennie CD, Millar RG. 2007. A deconvolution technique to separate bedload velocity from noisy data. *Journal of Hydraulic Engineering* **133(8)**: 845–856. DOI:10.1061/(ASCE)0733 9429(2007)133:8(845)

Rennie CD, Millar RG, Church MA. 2002. Measurement of bed load velocity using an acoustic Doppler current profiler. *Journal of Hydraulic Engineering* **128**: 473–483, DOI:10.1061/(ASCE)0733-9429(2002)128:5(473)

Rennie CD, Church MA. 2010. Mapping spatial distributions and uncertainty of water and sediment flux in a large gravel bed river reach using an acoustic Doppler current profiler. *Journal of Geophysical Research* **115**: F03035. DOI:10.1029/2009JF001556

Rhoads BL, Kenworthy ST. 1998. Time-averaged flow structure in the central region of a stream confluence. *Earth Surface Processes and Landforms* **23**: 171-191. DOI: 10.1002/(SICI)1096-9837(199802)23:2<171::AID-ESP842>3.0.CO;2-T

Rhoads BL, Kenworthy ST. 1999. On secondary circulation, helical motion and Rozovskii-based analysis of time-averaged two-dimensional velocity fields at confluences. *Earth Surface Processes and Landforms* **24**: 369-375. DOI: 10.1002/(SICI)1096-9837(199904)24:4<369::AID-ESP983>3.0.CO;2-F

Riley JD, Rhoads BL. 2012. Flow structure and channel morphology at a natural confluent meander bend. *Geomorphology* **163-164**: 84-98. DOI: 10.1016/j.geomorph.2011.06.011

Rozovskii IL. 1957. *Flow of Water in Bends of Open Channels*, Academy of Sciences of the Ukrainian SSR, Kiev (translated from Russian by the Israel Program for Scientific Translations, Jerusalem, 1961), 233 pp.

Shugar DH, Kostaschuk R., Best JL, Parsons DR, Lane SN, Orfeo O., Hardy RJ. 2010. On the relationship between flow and suspended sediment transport over the crest of a sand dune, Río Paraná, Argentina. *Sedimentology* **57**: 252–272. DOI: 10.1111/j.1365-3091.2009.01110.x

Sime LC, Ferguson RI, Church M. 2007. Estimating shear stress from moving boat acoustic Doppler velocity measurements in a large gravel bed river. *Water Resources Research* **43:** W03418. DOI:10.1029/2006WR005069.

Simpson MR, Oltman RN. 1993. Discharge-measurement system using an acoustic Doppler current profiler with applications to large rivers and estuaries. U.S. Geological Survey Water-Supply Paper 2395, 32 pp.

Simpson MR. 2001. Discharge measurements using a broad-band acoustic Doppler current profiler: U.S. Geological Survey Open-File Report 01-01, 134 pp.

Stacey MT, Monismith SG, Burau JR. 1999. Observations of Turbulence in a Partially Stratified Estuary. *Journal of Physical Oceanography* **29**: 1950–1970. DOI: 10.1175/1520-0485(1999)029<1950:OOTIAP>2.0.CO;2

Szupiany RN, Amsler ML, Best JL, Parsons DR. 2007. Comparison of fixed- and moving vessel measurements with an aDp in a large river. *Journal of Hydraulic Engineering* **133**: 1299–1309. DOI: 10.1061/(ASCE)0733-9429(2007)133:12(1299)

Szupiany RN, Amsler ML, Parsons DR, Best JL. 2009. Morphology, flow structure, and suspended bed sediment transport at two large braid-bar confluences. *Water Resources Research* **45***:* W05415. DOI:10.1029/2008WR007428

Teledyne RD Instruments 2009. *WinRiver II User's Guide*. Teledyne RD Instruments: San Diego, CA; 178 pp.

Topping DJ, Wright SA, Melis TS, Rubin DM. 2006. High-resolution monitoring of suspended-sediment concentration and grain size in the Colorado River using laser diffraction instruments and a three-frequency acoustic system. In *Proceedings of the 8th Federal Inter-Agency Sedimentation Conference*. Reno, Nevada; 539-546.

Wagner CR, Mueller DS. 2001. Calibration and validation of a two-dimensional hydrodynamic model of the Ohio River, Jefferson County, Kentucky. U.S. Geological Survey Water-Resources Investigation Report 01-4091. 40 pp.

Wall GR, Nystrom EA, Litten S. 2006. Use of an ADCP to compute suspended sediment discharge in the tidal Hudson River, New York. U.S. Geological Survey Scientific Investigations Report 2006-5055. 26 pp.

Wright SA, Kaplinski M. 2011. Flow structures and sandbar dynamics in a canyon river during a controlled flood, Colorado River, Arizona. *Journal of Geophysical Research* **116**: F01019, DOI:10.1029/2009JF001442

Tables

Table 1. VMT settings and parameters for generation of figures 5 through 11.

		Cross Section						*Plan View*			
Figure Number	**Horz. Grid Node Spacing (m)**	**Vert. Exag.**	**Vector Scale**	**Horz. Vector Spacing**	**Vert. Vector Spacing**	**Horz. Smooth Window**	**Vert. Smooth Window**	**Depth Range (m)**	**Vector Scale**	**Vector Spacing**	**Smoothing Window**
5	1	--	--	--	--	--	--	Full	1	15	1
6a	1	6	0.25	8	1	3	1	--	--	--	--
6b	1	6	0.3	8	1	3	1	--	--	--	--
6c	1	6	0.4	8	1	3	1	--	--	--	--
6d	1	6	0.4	8	1	3	1	--	--	--	--
6e	1	6	0.4	8	1	3	1	--	--	--	--
7a	0.25	--	--	--	--	--	--	Full	1.5	5	4
7b	0.25	--	--	--	--	--	--	Full	1.5	5	0
8a	0.25	5	0.12	12	2	0	0	--	--	--	--
8b	0.25	5	0.15	12	2	1	1	--	--	--	--
8c, 9c	0.25	5	0.18	12	2	8	2	--	--	--	--
9a	0.25	5	0.15	12	2	8	2	--	--	--	--
9b	0.25	5	0.15	12	2	8	2	--	--	--	--
10a	0.25	5	0.15	12	2	8	2	--	--	--	--
10b	0.25	5	0.15	12	2	8	2	--	--	--	--
11a	0.5	--	--	--	--	--	--	0 to 2.5m	2.2	15	8
11b	0.5	--	--	--	--	--	--	2.5m to 10m	1.5	15	8

Figure Captions

Figure 1: The VMT GUI interface with five sections including: i) data import; ii) graphics export, iii) processing options; iv) bathymetry export; and v) plotting options for both planform and cross-section views.

Figure 2: ADCP ensembles from section 2 of the Wabash-Embarras confluence (see Fig. 5) mapped to an average cross-section line in the VMT averaging procedure. Cross-section line (green line); ship tracks (blue lines); ensembles (blue circles); uniform mean cross-section grid nodes (black "+").

Figure 3: Schematic representation of the transect-averaging procedure employed by VMT during data processing.

Figure 4: Schematic diagram of the spatial-averaging procedures employed by VMT during data visualization with parameter settings available: horizontal smoothing window size, n_h, and a vertical smoothing window size n_v.

Figure 5: The planform distribution of depth-averaged flow velocity (in ms^{-1}) in the upper St. Clair River (MI, USA). Vector length and colour correspond to flow velocity. Vectors were obtained from the processing and averaging procedure in VMT. Inset figure shows multibeam bathymetry in the vicinity of cross-section 9 from Czuba et al. (2011).

Figure 6: Distribution of primary and secondary velocities (in ms^{-1}) for cross-section 9 of the upper St. Clair River (MI, USA). Secondary flows were computed using the zero net cross stream discharge definition. Panels show average flow fields for (a) one; (b) two; (c) four; (d) six and (e) eight ADCP transects. Interpolation and spatial averaging was held constant between panels.

Figure 7: The planform distribution of depth-averaged flow velocity (in ms^{-1}) at the confluence of the Wabash and Embarras Rivers (IL, USA) on May 23, 2006. Velocity vectors have been overlain on bathymetry data extracted from the ADCP data using VMT. Panels show the depth-averaged velocity with (a) no spatial averaging and (b) with data averaged with its nearest neighbour (horizontal smoothing window of 1).

Figure 8: The distribution of primary velocity (denoted by colour shading, in ms^{-1}) at cross-section 4 (see Figure 7), with secondary (applying a Rozovskii secondary circulation rotation) and vertical velocities superimposed as vectors illustrating the cross-stream velocity field, at the Wabash-Embarras confluence (IL, USA). The mapped velocities are from 4 individual transects and plotted

with (a) no smoothing; (b) light smoothing (horizontal smoothing window of 1 and a vertical smoothing window of 1); and (c) enhanced smoothing (horizontal smoothing window of 8 and a vertical smoothing window of 2). The view is looking downstream with inflow from the Embarras River on the right of the cross-section. The secondary and vertical velocities are scaled with no vertical exaggeration.

Figure 9: The distributions of streamwise and primary velocity (denoted by colour shading, in ms^{-1}) at cross-section 4 of the Wabash-Embarras confluence (IL, USA; see Figure 7), with superimposed vectors illustrating the vertical velocity and (a) the cross-stream velocity field; (b) the transverse velocity field computed using the zero net secondary discharge method; and (c) the transverse velocity field computed using the Rozovskii method. Mapped velocities are from 4 individual transects and are plotted with enhanced smoothing (horizontal smoothing window of 8 and a vertical smoothing window of 2). The view is looking downstream with inflow from the Embarras River on the right of the cross-section. The secondary and vertical velocities are scaled with no vertical exaggeration.

Figure 10: The distribution of (a) vertical velocity (denoted by colour shading, in ms^{-1}) and (b) acoustic backscatter (denoted by colour shading, in db) at cross-section 4 of the Wabash-Embarras river confluence (IL, USA; see Figure 7). Superimposed on each plot are vectors illustrating the vertical velocity and the transverse velocity field computed using the Rozovskii definition. Mapped velocities are from 4 individual transects and are plotted with enhanced smoothing (horizontal smoothing window of 8 and a vertical smoothing window of 2). The view is looking downstream with inflow from the Embarras River on the right of the cross-section. The secondary and vertical velocities are scaled with no vertical exaggeration.

Figure 11: The planform distribution of layer-averaged velocity (in ms^{-1}) for Clinton Lake in central Illinois (USA) for layers: (a) 0 to 2.5 m depth from the water surface and (b) below 2.5 m depth from the water surface. The raw ADCP data was gridded to a 0.50 m horizontal grid node spacing and averaged for reciprocal transects prior to visualization. Vector spacing in both figures is 7.5 m. Background imagery includes the distribution of surface water temperature (˚C) as measured by the ADCP thermistor. Temperature data were extracted using VMT (ASCII2GIS stand-alone utility) and gridded using kriging in ArcGIS®.

23x12mm (300 x 300 DPI)

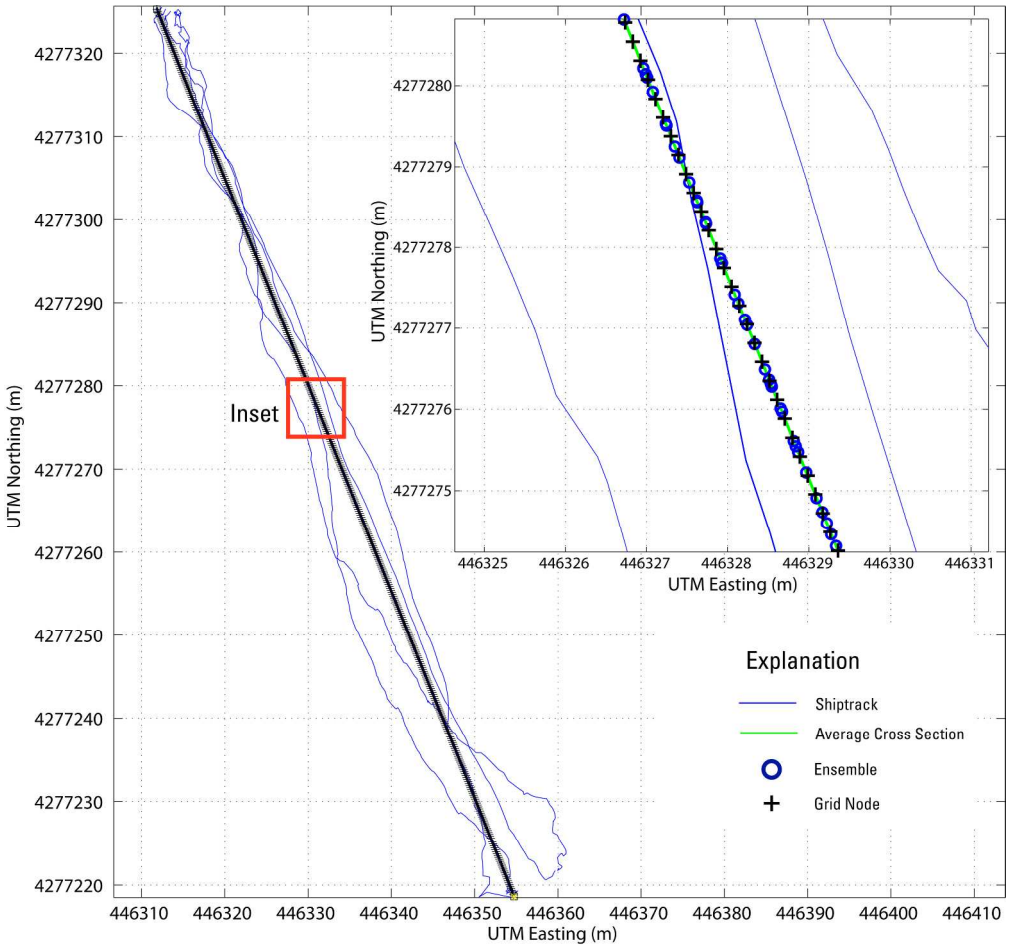

243x228mm (300 x 300 DPI)

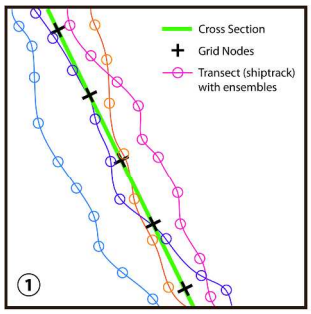

Step 1. Define the average cross section orientation and grid

Options:

1. Least-squares fit of data cloud
2. User-defined end points

Step 2. Project transect data to the cross section plane using an orthogonal translation

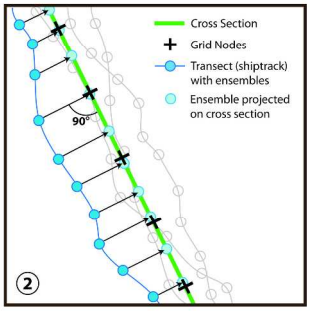

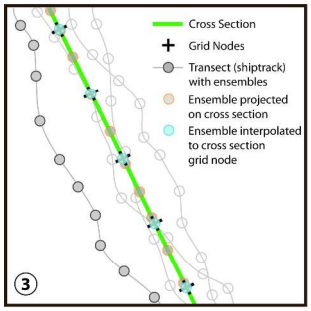

Step 3. Interpolate projected data to the cross section grid for each transect (no interpolation in vertical is required when using a vertical grid defined by the bin size)

Step 4. Compute arithmetic average of all transects at each grid node for basic variables (e.g. velocity components)

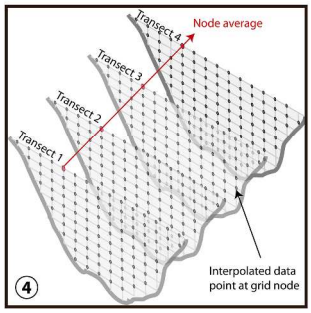

228x439mm (300 x 300 DPI)

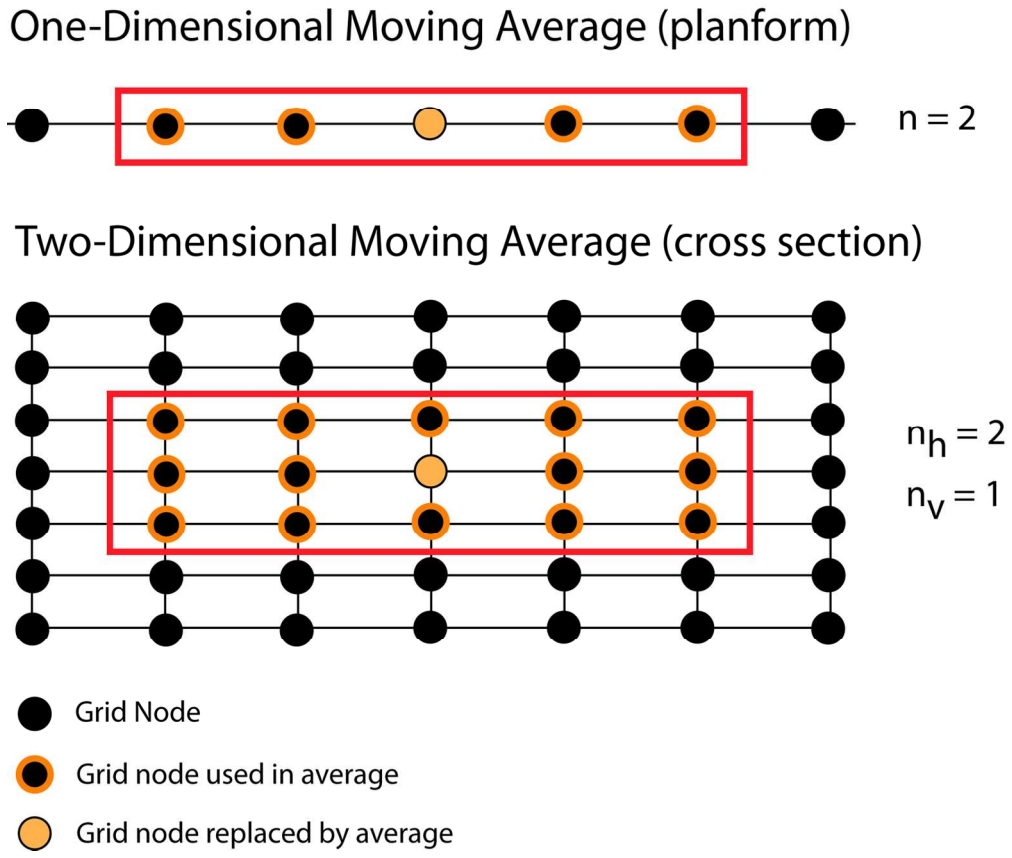

141x119mm (300 x 300 DPI)

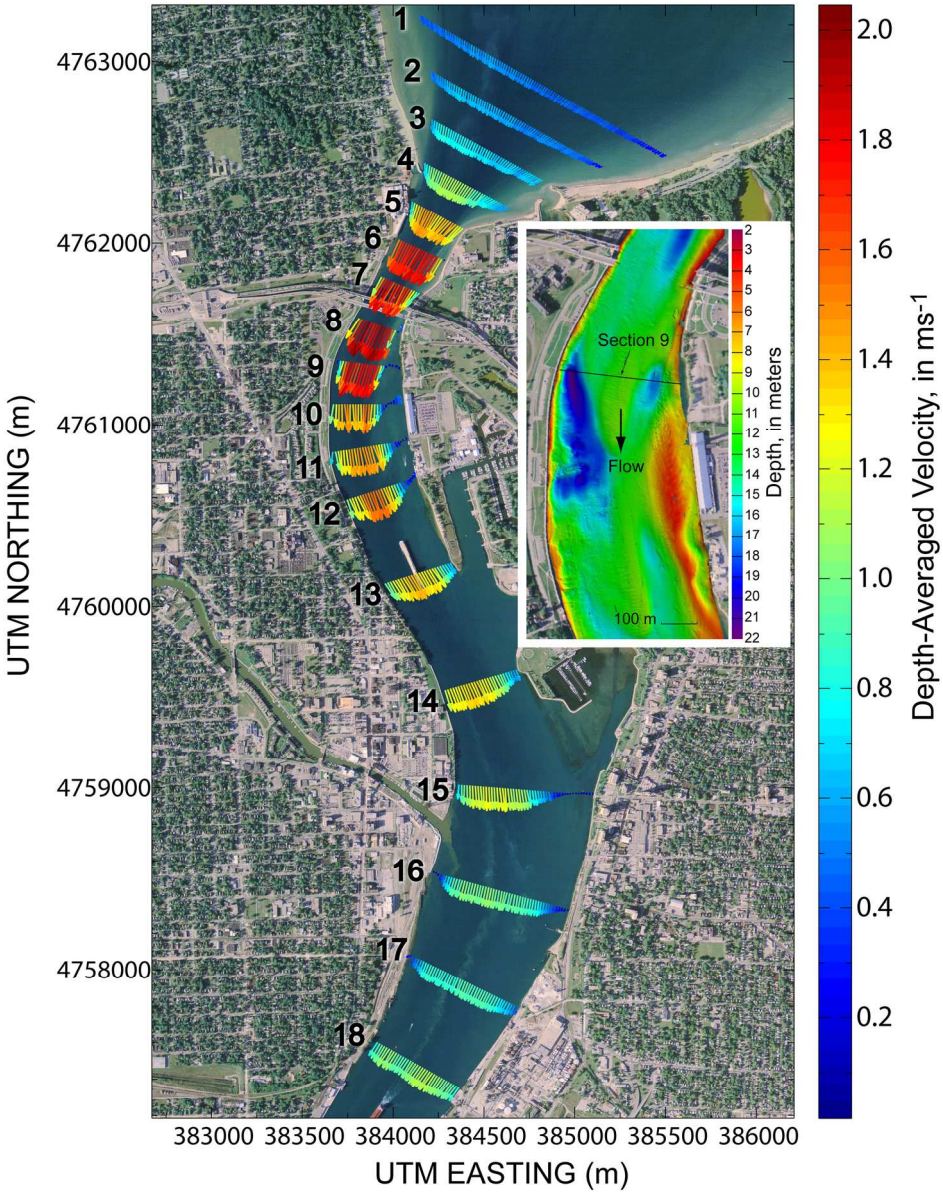

162x207mm (300 x 300 DPI)

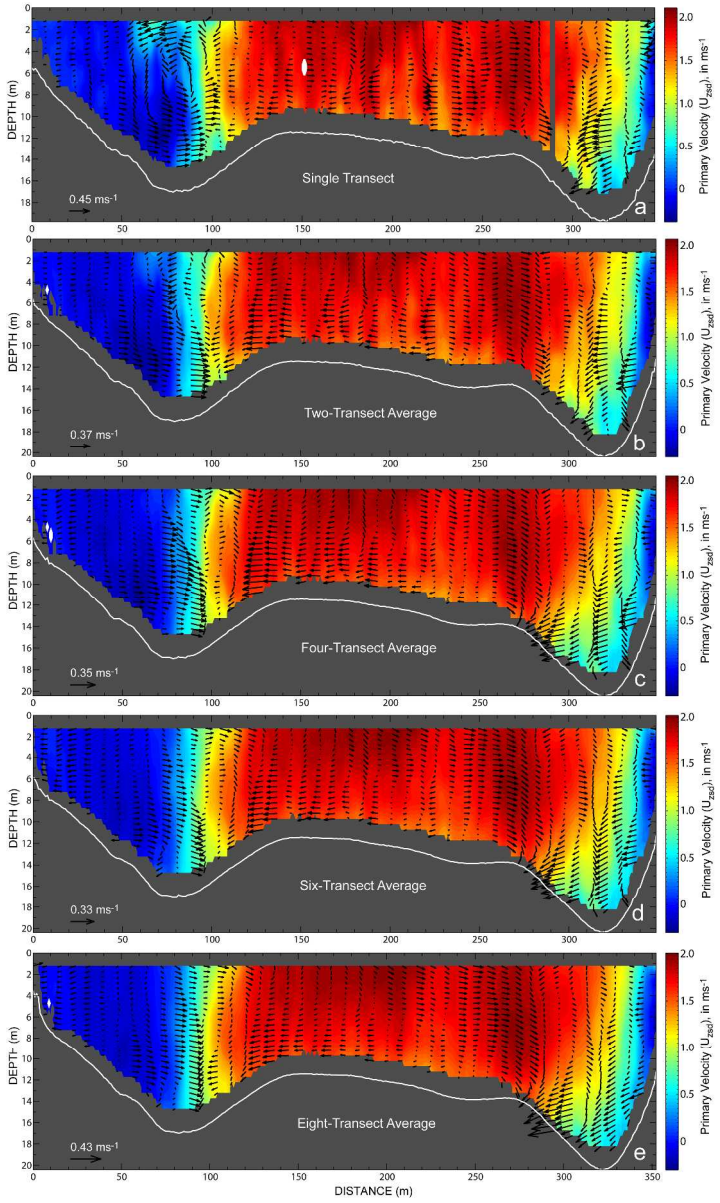

345x582mm (300 x 300 DPI)

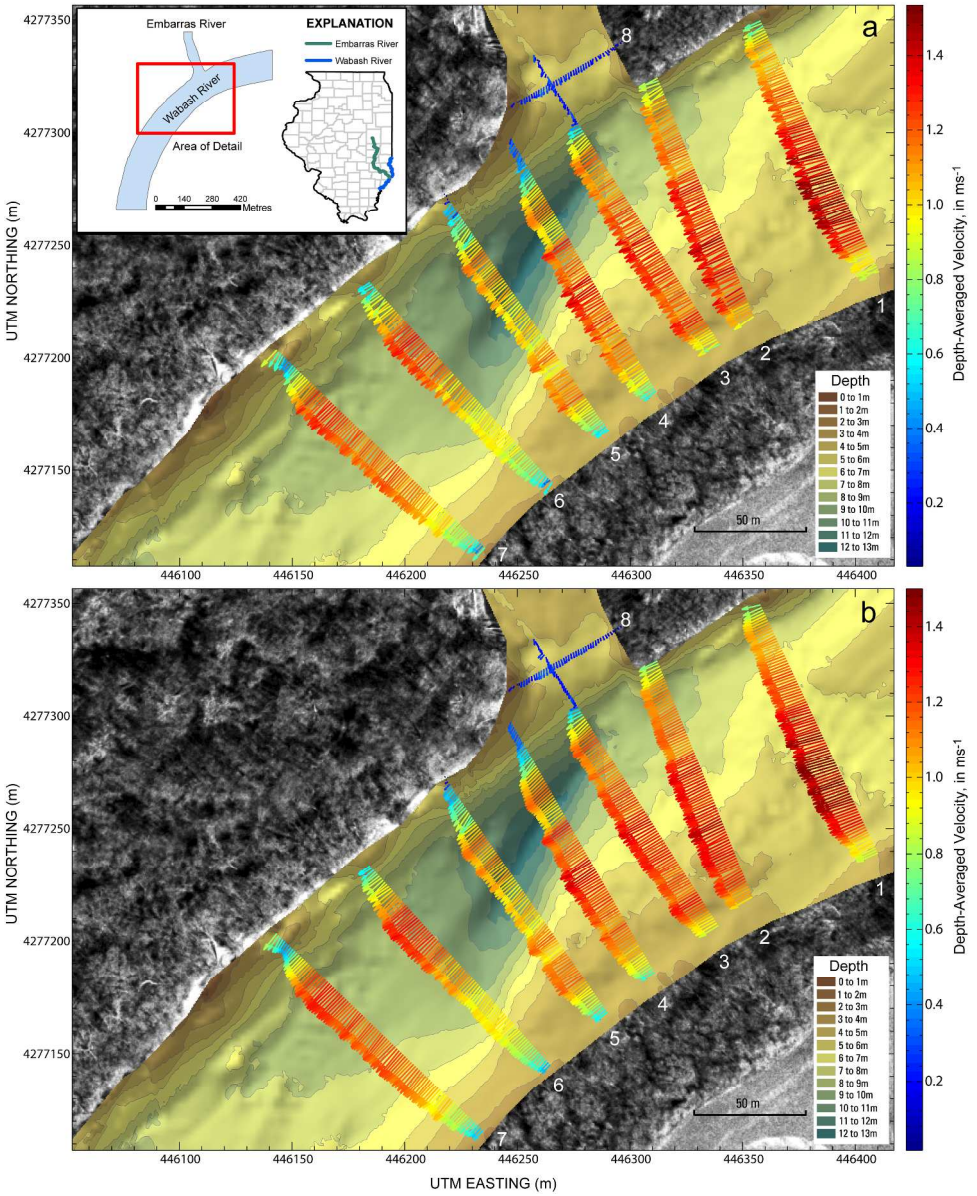

278x347mm (300 x 300 DPI)

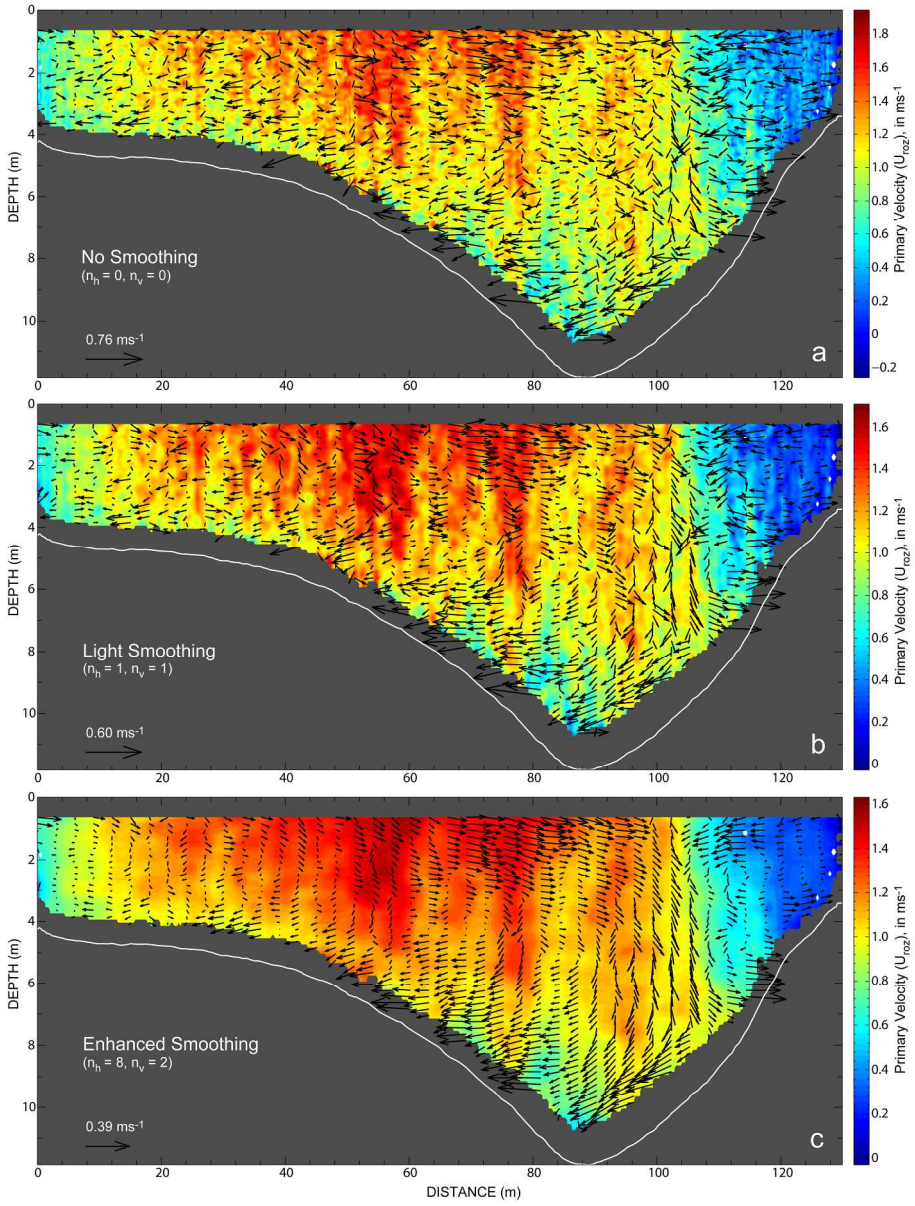

212x281mm (300 x 300 DPI)

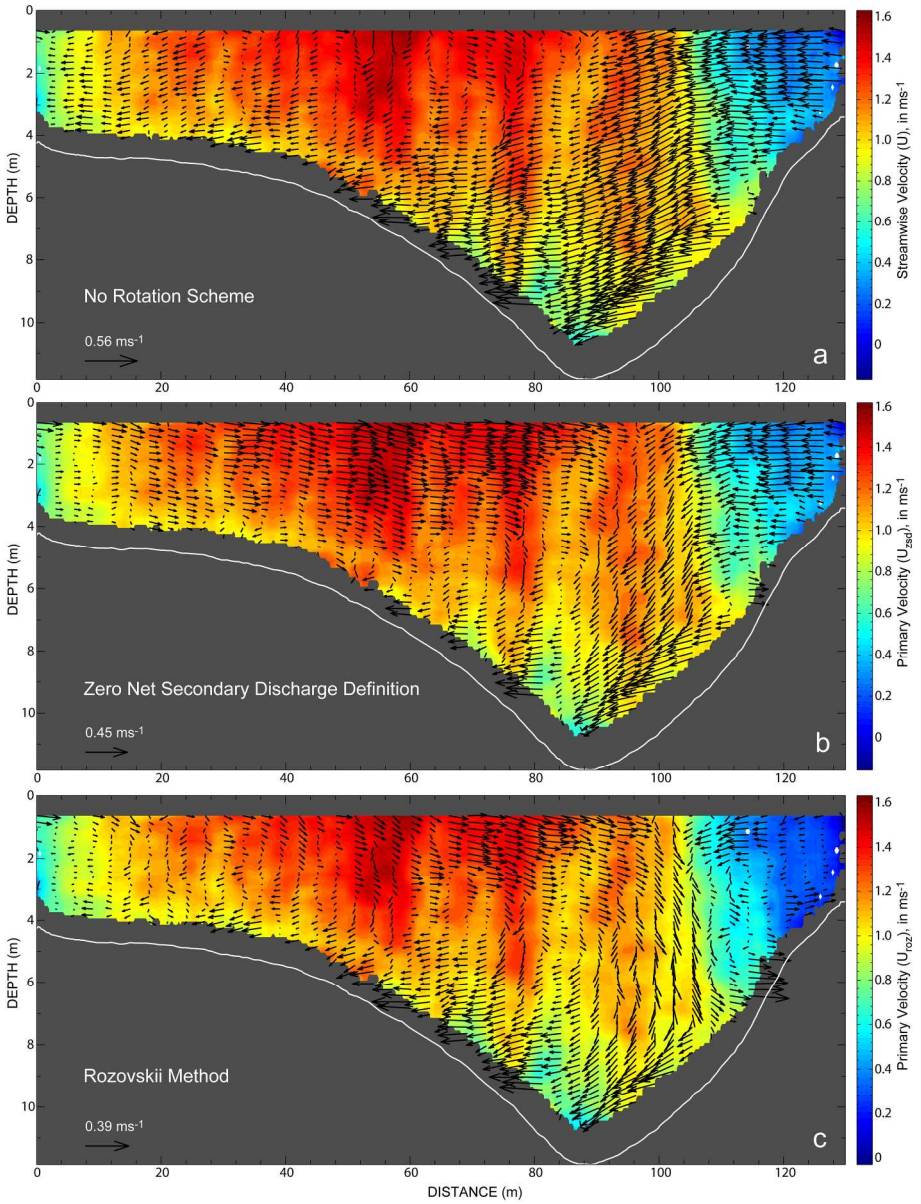

200x264mm (300 x 300 DPI)

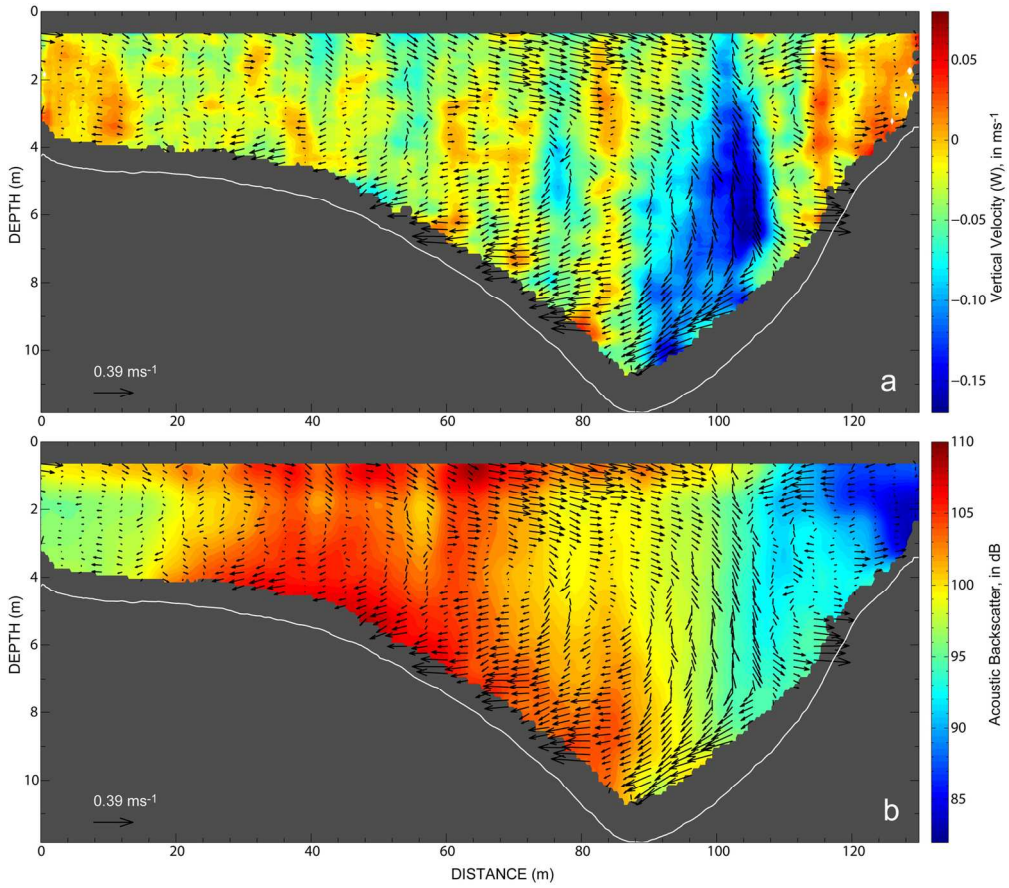

149x131mm (300 x 300 DPI)

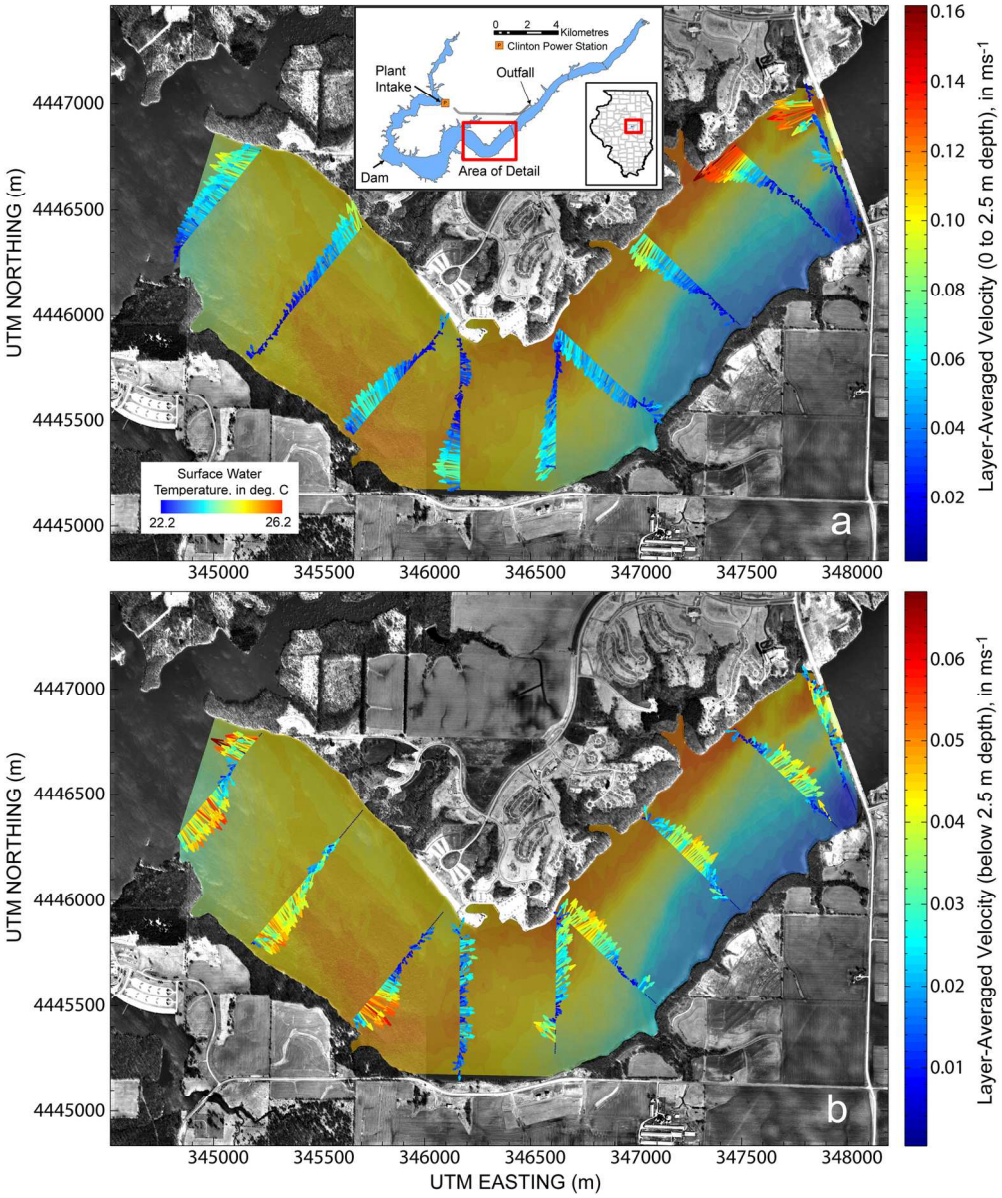

163x197mm (300 x 300 DPI)